Vibrations of acrylonitrile in N 1s excited states

Ilakovac, Vita; Carniato, Stephane; Gallet, Jean-Jacques; Kukk, Edwin; Horvatić, Davor; Ilakovac, Amon

Vibrations of acrylonitrile in N 1*s* excited states

V. Ilakovac,[1,2,*] S. Carniato,[1] J.-J. Gallet,[1] E. Kukk,[3] D. Horvatić,[4] and A. Ilakovac[4]
[1]*Laboratoire de Chimie Physique-Matière et Rayonnement, Université Pierre et Marie Curie, CNRS UMR 7614, F-75231 Paris, France*
[2]*Université de Cergy-Pontoise, F-95031 Cergy-Pontoise, France*
[3]*Department of Physics, University of Turku, FI-20014, Turku, Finland*
[4]*Department of Physics, University of Zagreb, Bijenicka c.32, P.O. Box 162, 10001 Zagreb, Croatia*
(Received 18 October 2007; published 30 January 2008)

The N 1*s* near edge x-ray absorption fine structure spectra of acrylonitrile gas are accurately reproduced by a complete *ab initio* multidimensional vibrational analysis. The role of π^*-orbital localization and hybridization on vibrations accompanying core excitation is discussed. Transition to the $\pi^*_\perp$(C=C−C≡N) delocalized orbital excites mostly stretching vibrations of the whole spinal column of the molecule. Promoting a core electron to the localized $\pi^*_\parallel$(C≡N) produces C≡N stretching vibration combined with two strong bending modes of the C−C≡N end of the molecule, related to the change of carbon hybridization.

DOI: 10.1103/PhysRevA.77.012516 PACS number(s): 33.20.Rm, 31.15.E−, 33.20.Tp, 33.70.Ca

I. INTRODUCTION

The dynamics of molecular motion under resonant core-electron excitation by synchrotron radiation is becoming an important field opening possibilities for light-assisted reactions, dissociation, or targeted heating. This can be used in different fields, such as organic electronics or even medical radiotherapy [1]. Vibrational fine structure is one of the most striking features accompanying electronic excitation of molecules. It was observed more than 30 years ago [2] in core-hole photoelectron spectra. It permits insight into the complex dynamics of molecular excitation. The field is rapidly expanding thanks to new synchrotron sources of radiation, with high flux and high resolution, permitting the resolution of structures which are even less than a few meV apart. At the same time, the theoretical improvement, allowing calculation of geometries, frequencies, and potential functions of initial and final (core-hole excited) states, makes realistic interpretations possible.

It is now well established that under core-hole photoexcitation or photoionization a molecule exhibits as a major deformation a shortening and/or elongation of its chemical bonds. Nice examples are studies of photoexcited diatomic NO and CO molecules [3,4], or photoionized centrosymmetric molecules, such as methane [5], where due to high symmetry only stretching vibrations can be excited. These modes have energy quanta of more than 100 meV, usually larger than the mean lifetime broadening of a core-hole excitation of light elements, and can easily be resolved. Besides excitation of the same element on chemically nonequivalent sites [6–9], and excitations to different orbital states [3,4], they are a dominating contribution to the fine structure of spectra of polyatomic molecules with lower symmetry [10]. On the other hand, under core-hole excitation a molecule can exhibit an electronic redistribution or even rehybridization which creates a tendency to change angles. In this way bending oscillations are introduced, like in N 1*s* excited N_2O [6] or benzonitrile [11,12], and C 1*s* excited ethylene [7], benzene [8], or CH_3 free radical [13]. Even the torsion degrees of freedom can be excited [14]. Bending and torsion modes have lower frequencies, a few tens of meV, frequently smaller than the mean lifetime broadening, and thus cannot be resolved even if the experimental resolution is high. Combined with stretching modes, they can broaden the spectral structure and apparently deteriorate the resolution [6,11,12,14].

Acrylonitrile (see Fig. 1) is a model molecule for vibrations accompanying core-hole excitations, because it has many vibrational modes of different character. Among its 15 vibrational modes, six of them are stretchings, three are bendings, one is torsion, and others are of wagging, rocking, and deformation characters [15]. This paper shows that, from this richness of vibrations, accommodating a core electron in the two lowest unoccupied π^* states of different symmetry will not excite the same set of vibrational modes. A complete multidimensional vibrational analysis is done for the ground state and the two core-excited states of the molecule. A calculation of Franck-Condon factors for bending modes presenting asymmetric-double-well potentials in the core-excited state is performed.

The paper is organized as follows: Experimental details are given in Sec. II, and models used for calculation of Franck-Condon factors in Sec. III. In Sec. IV, presentation of results, and discussion, are separated into three parts, the first concerning the ground state, the second and third concerning the two π^*-excited states.

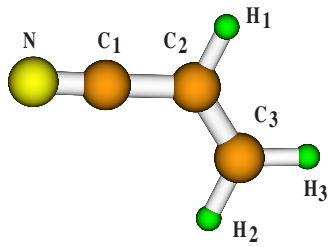

FIG. 1. (Color online) $H_2C=CHC\equiv N$, acrylonitrile molecule.

*ilakovac@ccr.jussieu.fr

II. EXPERIMENT

The experimental measurements were performed at the undulator beamline I411 at the MAX II storage ring in Lund, Sweden. The beamline is equipped with a Zeiss SX-700 modified plane grating monochromator [16] and an end station specifically built for the study of gases and soft molecular materials [17]. The near edge x-ray absorption fine structure (NEXAFS) spectrum was recorded in the Auger yield mode using a Scienta SES-200 electron analyzer. An integration window of electron kinetic energy between 356 and 385 eV with the pass energy of 300 eV was used. This includes the two *KLL* Auger transitions. The energy calibration was done with the help of the N_2 NEXAFS spectrum [18]. Under these experimental conditions the photon energy resolution was better than 70 meV. Intensity was normalized by the photon flux measured using a photodiode. Acrylonitrile was purchased from Aldrich (99%, anhydrous) and purified by several freeze-pump-thaw cycles. The target gas was introduced at room temperature into a differentially pumped gas cell and the pressure was maintained at 10^{-6} mbar during measurement.

III. CALCULATIONS

The electronic absorption spectrum is monitored by the matrix elements of the dipole momentum operator, $\Omega_{fi}=\langle\chi_{v_f}\Psi_f|\mu|\chi_{v_i}\Psi_i\rangle$, where χ and Ψ are the nuclear and electronic wave functions in the initial i and final f states, and v_i and v_f are the corresponding set of quantum numbers. In the Franck-Condon approximation, the electronic dipole matrix elements, $\mu_{fi}=\langle\Psi_f|\mu|\Psi_i\rangle$, are independent of nuclear displacements, at least in the region covered by the spatial extension of χ_{v_i}. This yields to the Franck-Condon amplitudes

$$\Omega_{fi}\sim\mu_{fi}\langle\chi_{v_f}|\chi_{v_i}\rangle. \tag{1}$$

A. Direct calculation of Franck-Condon factors

The natural basis for the calculations of the overlaps $\langle\chi_{v_f}|\chi_{v_i}\rangle$ is the basis of normal coordinates. A molecule with N atoms has $\mathcal{M}=3N-6$ vibrational modes ($3N-5$ if it is linear). The normal coordinate corresponding to the vibrational mode a is calculated from Cartesian coordinates by rescaling by the square root of the mass of the corresponding atom and rotating by the unitary matrix U,

$$\sqrt{m_a}(x_a-x_{a0})=\sum_{j=1}^{\mathcal{M}}U_{aj}q_j. \tag{2}$$

Vibrational wave functions corresponding to the ground state (χ_{v_i}) and the excited state (χ_{v_f}) can be obtained from $\mathcal{M}$ one-dimensional Schrödinger equations for $V_a(q_a)$, the potential in the direction of the normal coordinate q_a. Here q_a represents displacement from the ground-state geometry (labeled by $q=0$) in the direction of the ground-state normal coordinate of the mode a.

The multidimensional Schrödinger equation is then simplified to a set of $\mathcal{M}$ equations,

$$\frac{\partial^2\psi_{n_a}}{\partial q_a^2}+V_a(q_a)\psi_{n_a}=E_{n_a}\psi_{n_a}, \tag{3}$$

where n_a is a quantum number of the wave function of the coordinate a. The calculation should be done for the ground-state potentials, $V_a^{\mathrm{gs}}(q_a)$, and the excited-state potentials, $V_a^{\mathrm{exc}}(q_a)$. The approximation of identical normal coordinates in the ground and excited states is used to obtain $\mathcal{M}$ one-dimensional potentials of the excited state.

Finally, the ground state characterized by quantum vibrational numbers $v_i=(n_1,n_2,\ldots)$ is represented as a product

$$\chi_{v_i}=\prod_{a=1}^{\mathcal{M}}\psi_{n_a}(q_a), \tag{4}$$

and for the final state $v_f=(n_1',n_2',\ldots)$,

$$\chi'_{v_f}=\prod_{a=1}^{\mathcal{M}}\psi'_{n'_a}(q_a). \tag{5}$$

For excitations of the individual mode a, Franck-Condon (FC) amplitudes are defined as overlaps between the ground-state (ψ_{n_a}) and excited-state ($\psi'_{n'_a}$) functions,

$$\mathcal{A}_{\mathrm{FC}}(n_a\rightarrow n_a')=\langle\psi'_{n'_a}|\psi_{n_a}\rangle. \tag{6}$$

The probability of the transition from the initial vibrational state $(n_1,n_2,\ldots)$ to the final vibrational state $(n_1',n_2',\ldots)$, is then a product of the FC factors which are themselves squares of the FC amplitudes,

$$I(n_1\rightarrow n_1',n_2\rightarrow n_2',\ldots)=\prod_{a=1}^{\mathcal{M}}|\langle\psi'_{n'_a}|\psi_{n_a}\rangle|^2. \tag{7}$$

The vibrational energy needed for this transition is

$$E(n_1\rightarrow n_1',n_2\rightarrow n_2',\ldots)=\sum_{a=1}^{\mathcal{M}}[E(n_a')-E(n_a)]. \tag{8}$$

B. Linear coupling model

Overlaps of vibrational wave functions can easily be calculated in the case of harmonic potentials with the same curvature ($\omega_a'=\omega_a$) but displaced along the normal coordinates [usually called the linear coupling (LC) model]. For the normal coordinate a, the displacement of the electronic initial state potential (V_a^{gs}) and the excited-state potential (V_a^{exc}) is proportional to the gradient of the excited-state potential for the ground-state equilibrium geometry ($q=0$),

$$\delta q_a=\frac{1}{\omega_a^2}\frac{\partial V_a^{\mathrm{exc}}}{\partial q_a}\bigg|_{q=0}. \tag{9}$$

The coupling constant can be calculated as

$$S_a=\frac{\omega_a\delta q_a^2}{2\hbar}, \tag{10}$$

leading to the analytic expression of Franck-Condon amplitudes [19–21]: For $n_a>n_a'$,

TABLE I. Interatomic distances and angles of acrylonitrile in its electronic ground state (calculated and experimental), relaxed geometry in the $\pi^*_\perp$-excited state, and relaxed geometry in the $\pi^*_\parallel$-excited state. Values for acrylaldehyde radical (CH_2CHCO), acrylaldehyde (CH_2CHCHO), and acrylonitrile adsorbed on Si(100) by cycloaddition [38–42], are noted for comparison.

	Ground state			$\pi^*_\perp$-excited		$\pi^*_\parallel$-excited		Si(100)
Distances (Å)	Calc.	Expt. [33]	Expt. [34]	state	CH_2CHCO	state	CH_2CHCHO [34]	cycloadded
$N(O)\equiv C_1$	1.154	1.164	1.167	1.171	1.166	1.194	1.217	1.291
C_1-C_2	1.428	1.426	1.438	1.335	1.336	1.469	1.484	1.491
$C_2=C_3$	1.334	1.339	1.343	1.469	1.491	1.335	1.345	1.347
C–H	1.082	1.086	1.130	1.08	1.08	1.08	1.13	1.08
Angles (deg)								
$C_1C_2C_3$	122.7	122.6	121.7	126.4	126.1	120.4	120.3	122.7
$C_2C_3H_2$	121.6	121.7	120	121.6	121.6	120.7	122	121.4
$N(O)C_1C_2$	178.7		178	179.1	179.3	128.7	123.3	120.6

$$\langle \psi_{n'_a} | \psi_{n_a} \rangle = e^{-S_a/2} S_a^{(n_a-n'_a)/2} \sqrt{\frac{n'_a!}{n_a!}} L_{n'_a}^{n_a-n'_a}; \tag{11}$$

for $n_a < n'_a$,

$$\langle \psi_{n'_a} | \psi_{n_a} \rangle = (-1)^{n'_a-n_a} \langle \psi_{n_a} | \psi_{n'_a} \rangle. \tag{12}$$

Here, $L_{n'_a}^{n_a-n'_a}$ is the associated Laguerre polynomial,

$$L_{n'_a}^{n_a-n'_a} = \sum_{j=0}^{n'_a} \frac{n_a!\,(-S_a)^j}{(n'_a-j)!\,(n_a-n'_a+j)!\,j!}. \tag{13}$$

If the thermal excitation is negligible compared to the vibrational excitation energy, then $n_a=0$, and the overlap simplifies to

$$\langle \psi_{n'_a} | \psi_0 \rangle = \frac{S_a^{n'_a/2}}{\sqrt{n'_a!}} e^{-S_a/2}. \tag{14}$$

In the case where $\omega_a \neq \omega'_a$, the shift of the excited potential in normal coordinates can be obtained by Eq. (9) where ω_a should be replaced by ω'_a and the coupling constant changes to [22]

$$S'_a = \frac{\omega'_a (\delta q'_a)^2}{\hbar\left(1+\frac{\omega'_a}{\omega_a}\right)}. \tag{15}$$

Concerning symmetric potentials, the LC model gives a wrong estimation of the FC factors. As the gradient of the excited-state potential expressed in Eq. (9) is zero at $q=0$, all $\mathcal{A}_{FC}(n\neq 0)$ have zero value. This is not the case if $\omega'_a \neq \omega_a$, for the overlap of all functions of the same symmetry is different from zero. Knowing ω_a and ω'_a, the correction can be made by the method proposed by Katriel [23]. Here we present the expression for the FC factors only for excitations from $\psi_a(n=0)$ to $\psi'_a(n')$,

$$\mathcal{A}_{FC}(0\rightarrow n') = (n'!)^{1/2}\left(\frac{2(\omega\omega')^{1/2}}{\omega+\omega'}\right)\sum_{j=0}^{n'} \frac{1}{\left(\frac{1}{2}(n'-j)\right)!\,j!} \times \left(\frac{\omega-\omega'}{2(\omega+\omega')}\right)^{1/2(n'-j)} \left(\frac{2(\omega\omega')^{1/2}}{\omega+\omega'}\right)^{j}. \tag{16}$$

Equation (16) is restricted to even values of both n' and j.

C. Calculation details

The calculations were done using the density functional theory (DFT) with Becke three-parameter hybrid exchange [24] and the Lee-Yang-Parr gradient-corrected correlation functional [25] (B3LYP) implemented in the GAMESS (U.S.) program [26]. Recent works using DFT/B3LYP implemented programs show that this method gives realistic interatomic distances and accurate photoionization [27,28] and photoexcitation [11–13] energies of light elements, such as carbon, nitrogen, and oxygen. The IGLOO-III basis set [29] is used for the nitrogen and the 6-311G** basis set [30] for carbon and hydrogen atoms. The core-excitation energies are computed for a triplet final state using the Δ Kohn-Sham (ΔKS) approach. The singlet-triplet correction is calculated by the sum method of Ziegler, Rauk, and Baerends [31] and the relativistic correction of 0.3 eV for nitrogen [32] has been included. The geometry optimizations were performed for initial and final states.

The resolution of the Schrödinger equation in normal coordinates is done numerically by the finite difference method.

IV. RESULTS AND DISCUSSION

A. Ground state

In the electronic ground state, acrylonitrile is a planar noncentrosymmetric molecule, belonging to symmetry point group C_S (see Fig. 1). The calculated interatomic distances and angles are compared to experimental values [33,34] in Table I. Calculated and experimental values are less than 1% apart.

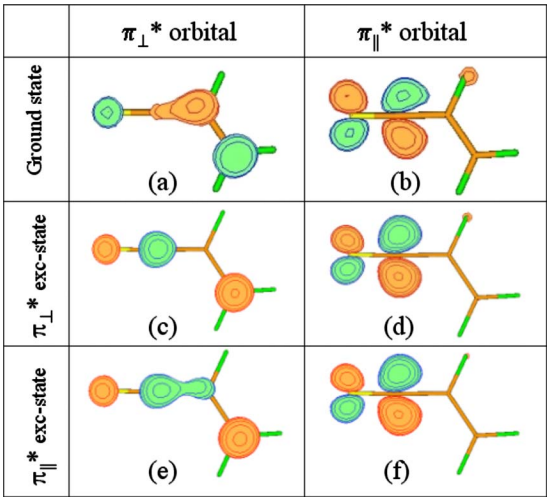

FIG. 2. (Color online) $\pi_{\perp}^{*}$ (left-hand side) and $\pi_{\parallel}^{*}$ (right-hand side) orbitals in the ground state (upper), $\pi_{\perp}^{*}$-excited state (middle), and the $\pi_{\parallel}^{*}$ (lower) state.

The electronic ground-state configuration of its 20 valence electrons has been determined using photoelectron spectroscopy [35]. For the outermost valence molecular orbitals perpendicular to the plane of the molecule, the π states are delocalized along the C=C−C≡N chain due to conjugative interaction between the C=C bond and the C≡N bond. This conjugation gives rise to two bonding, $1a''$, $2a''$, and two antibonding, $3a''$, $4a''$, orbitals. The lowest unoccupied molecular orbital (LUMO), $3a''$, is shown in Fig. 2(a). In the following it will be labeled $\pi_{\perp}^{*}$(C=C−C≡N), or in short, $\pi_{\perp}^{*}$. The π states of the C≡N group which lie in the molecular plane are mostly localized on this group, and lead to one bonding orbital, $12a'$, and one antibonding orbital, $13a'$ (LUMO+1). The second will be labeled $\pi_{\parallel}^{*}$(C≡N), or in short, $\pi_{\parallel}^{*}$ [see Fig. 2(b)]. The next unoccupied orbital (LUMO+2) is $4a''$ [equally $\pi_{\perp}^{*}$(C=C−C≡N)], and others are of the σ^{*} type.

Acrylonitrile has 15 normal vibrational degrees of freedom. There are 11 vibrations in the plane of the molecule (A'), and four are out of plane, belonging to the A'' irreducible representation. The corresponding calculated wave numbers (σ in cm^{-1}) and energies ($\hbar\omega$ in eV) are compared to experimental values [15,36] in Table II (ground state). The experimental values for modes $a=13,14,15$ are given only for the liquid phase. Wave numbers are calculated from the first vibrational quanta

$$\hbar\omega = E_1 - E_0, \tag{17}$$

where E_0 and E_1 are the first two eigenvalues of the Schrödinger equation for the potential of the mode a. The calculated values are higher for 1%–3% for modes with a wave number greater than 1000 cm^{-1}, and 4%–8% for a smaller σ. Calculation of the frequency using the gradient of

TABLE II. Vibrational modes in the ground state, and $\pi_{\perp}^{*}$- and $\pi_{\parallel}^{*}$-excited states. First two columns: Number (a), symmetry, and nature of the vibration. s, d, r, b, w, t, are for stretching, deformation, rocking, bending, wagging, and torsion. Ground state: Experimental (σ_{expt}, Refs. [15,36]), calculated (σ) wave number in cm^{-1}, and $\hbar\omega$ in meV, defined by Eq. (17). $\pi_{\perp}^{*}$-excited state: $\hbar\omega_{\perp}$, frequency change relative to the ground state ($\Delta\omega_r$), and the first three FC factors for each mode. $\pi_{\parallel}^{*}$-excited state: $\hbar\omega_{\parallel}$, $\Delta\omega_r$ except for symmetric- (*sdw*) and asymmetric-double-well (*adw*) potentials, the quantum number of the most excited vibrational state (m), the first three FC factors, and, for *adw*, the FC factor of the most excited vibrational state.

		Ground state			$\pi_{\perp}$-excited state					$\pi_{\parallel}$-excited state						
a	Character	σ_{expt}	σ	$\hbar\omega$	$\hbar\omega_{\perp}$	$\Delta\omega_r$(%)	FC(0)	FC(1)	FC(2)	$\hbar\omega_{\parallel}$	$\Delta\omega_r$(%)	m	FC(0)	FC(1)	FC(2)	FC(m)
A'	(in plane)															
1	C–H s	3125	3235	402	401	0	1.00	0.00	0.00	403	0	1	1.00	0.00	0.00	
2	C–H s	3078	3008	374	380	+2	1.00	0.00	0.00	357	−4	1	0.97	0.01	0.00	
3	C–H s	3042	3102	385	389	+1	1.00	0.00	0.00	383	−1	1	1.00	0.00	0.00	
4	C≡N s	2239	2290	285	256	+10	0.77	0.20	0.03	262	−8	1	0.68	0.25	0.06	
5	C=C s	1615	1655	206	175	−15	0.65	0.28	0.06	194	−6	1	0.96	0.04	0.00	
6	CH_2 d	1416	1437	179	176	−2	0.95	0.05	0.00	175	−2	1	0.99	0.01	0.00	
7	CH r	1282	1317	164	157	−4	0.89	0.11	0.00	165	+1	1	0.95	0.05	0.00	
8	CH_2 r	1096	1112	138	133	−4	0.79	0.19	0.02	127	−8	1	0.88	0.11	0.00	
11	C–C s	869	917	109	111	+2	0.67	0.28	0.05	105	−4	1	0.97	0.03	0.00	
13	C=C−C b	570[a]	580	72	81	+13	0.96	0.04	0.00	89	*adw*	8	0.00	0.00	0.01	0.50
15	C−C≡N b	242[a]	263	33	22	−33	0.85	0.14	0.01	59	*adw*	6	0.00	0.01	0.00	0.44
A''	(out of plane)															
9	CH_2=CH w	972	1028	128	103	−20	0.99	0.00	0.01	128	0	1	1.00	0.00	0.00	
10	CH_2=C w	954	1021	127	98	−23	0.99	0.00	0.01	131	+3	1	0.99	0.00	0.00	
12	C=C t	683	722	89	47	−47	0.95	0.00	0.05	92	+3	1	1.00	0.00	0.00	
14	C−C≡N b	362[a]	375	47	28	−40	0.97	0.00	0.03	26	*sdw*	1	0.96	0.00	0.04	

[a]Liquid phase.

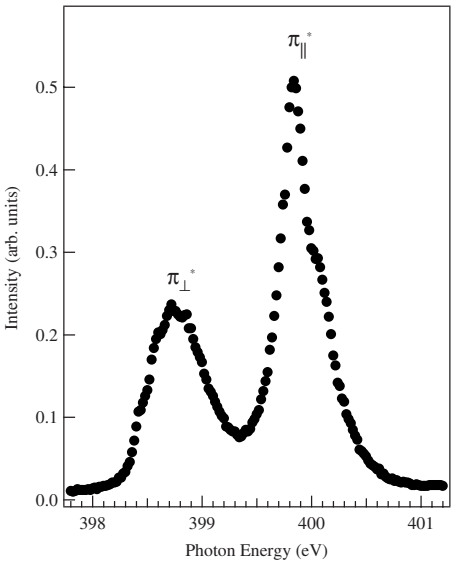

FIG. 3. Experimental N *K*-edge NEXAFS spectrum of acrylonitrile molecule.

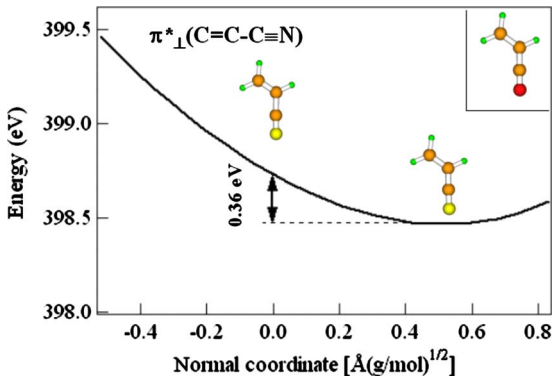

FIG. 4. (Color online) Potential leading to the optimized geometry in the $\pi_{\perp}^*$-excited state, from the vertically attained (at $q=0$) $\pi_{\perp}^*$-excited state, shown along a direct path and in terms of normal coordinate distance between the two states. The molecule with relaxed geometry in the excited state is shown in the minimum of the potential. The CH_2CHCO molecule of similar geometry is shown in the inset.

the potential close to its minimum, for σ smaller than 1000 cm^{-1}, gives results closer to the experimental values, with relative differences better than 3%. This correction is not very important as it induces a shift of at most 30 meV of the whole vibrational progression.

B. Core excited states

The NEXAFS spectrum for photon energies near the N *K*-edge is shown in Fig. 3 for the two first resonances. Two strong and distinct peaks can be seen in the spectrum, centered at 398.75 eV and 399.71 eV, with photon energy resolution of 70 meV. Previous work reports very close values, 398.68 eV and 399.79 eV, measured by electron energy loss spectroscopy [37]. Vertical ΔKS transition energies corresponding to N $1s \rightarrow \pi^*$ are calculated as the energy difference between the ground state and the π^*-excited state without changing the molecular geometry. The values for the N $1s \rightarrow \pi_{\perp}^*$ and N $1s \rightarrow \pi_{\parallel}^*$ transitions, 398.73 eV and 399.75 eV, respectively, are in excellent agreement with experimental values.

1. Transition to the $\pi_{\perp}^*$(C=C−C≡N)

When a N 1*s* electron is promoted to the $\pi_{\perp}^*$(C=C−C≡N) molecular orbital, there is a net electron transfer to the nitrogen part of the molecule in the $\pi_{\perp}$(C=C−C≡N) bonding (occupied) orbital, in order to screen the core hole. Similar density redistribution is visible in the antibonding $\pi_{\perp}^*$ orbital [see Fig. 2(c)], occupied then by one electron participating in the screening.

The optimized geometry in the $\pi_{\perp}^*$-excited state has an energy 0.36 eV lower than the ground-state geometry (see Fig. 4). The relaxed geometry in this excited state is similar to that of the molecule whose nitrogen is replaced by an oxygen (see Table I), because in both cases the extra electron is accommodated in the LUMO orbital. The most important deformations, relative to the molecule in the ground-state geometry, are 9.3 pm shortening of the C–C bond, 7.3 pm lengthening of the C=C bond, and 1.7 pm extension of the C≡N bond. The tendency of shortening and/or lengthening in this excited state indicates that vibrations which are excited are mostly of stretching character.

Normal coordinate multidimensional analysis of the $\pi_{\perp}^*$-excited potential surface gives 15 single-well potentials. Potentials of out-of-plane modes are centered at $q_a=0$ for symmetry reasons. In-plane modes have more or less shifted potential curves.

The ground and the $\pi_{\perp}^*$-excited-state potentials for the second most excited, C–C stretching ($a=11$), vibrational mode is shown in Fig. 5 together with the corresponding eigenvalues and eigenfunctions. The FC factors are indicated on the right-hand side of the first three vibrational eigenfunctions in the excited state. ψ_0' is excited with the probability 0.67, while the probability of transitions to ψ_1' and ψ_2' are 0.28 and 0.05, respectively.

Table II ($\pi_{\perp}^*$-excited state) reports excited-state first vibrational quanta ($\hbar\omega_{\perp}=E_{a1}'-E_{a0}'$), the relative difference of frequencies in the excited and ground states ($\Delta\omega_r$), and the first three FC factors, obtained by direct calculation for each mode a. $\Delta\omega_r$ is calculated as

$$\Delta\omega_r = \frac{\omega_a' - \omega_a}{\omega_a}. \tag{18}$$

It is interesting to note that four out-of-plane modes and two in-plane modes are subject to frequency softening of more than 10%, while one has hardening of 13%. Modifying the curvature of the potential changes the extension of the wave functions and can have influence on the FC factors.

Examination of the FC factors in Table II shows that for all modes the transition to the state $n'=0$ has the highest probability. But for many in-plane modes, the probability to excite the first harmonic is, however, important, going to almost 30% for C=C and C–C stretchings. As the first har-

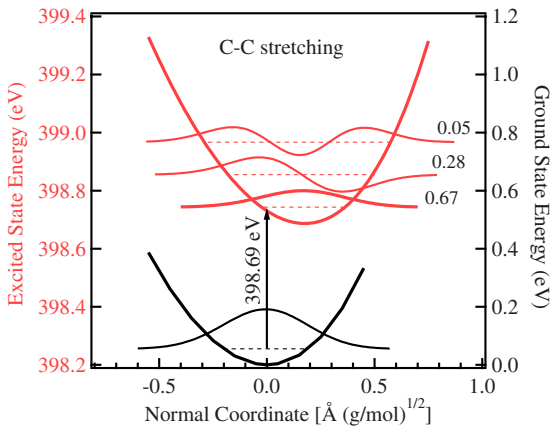

FIG. 5. (Color online) Ground state (full black line), $\pi^*_\perp$-excited-state [full gray (red) line] potential, and corresponding wave functions, for the second most excited, C–C stretching, vibrational mode ($a=11$). The ground-state energy scale is on the right-hand side, and the excited state at the left-hand vertical axis. Horizontal dashed lines indicate corresponding eigenvalues. The arrow indicates a vertical transition (at $q=0$) between ψ_0 and ψ'_0. Probabilities of transitions to the first three vibrational states are indicated. Wave functions with higher excitation probability are drawn by a thicker line.

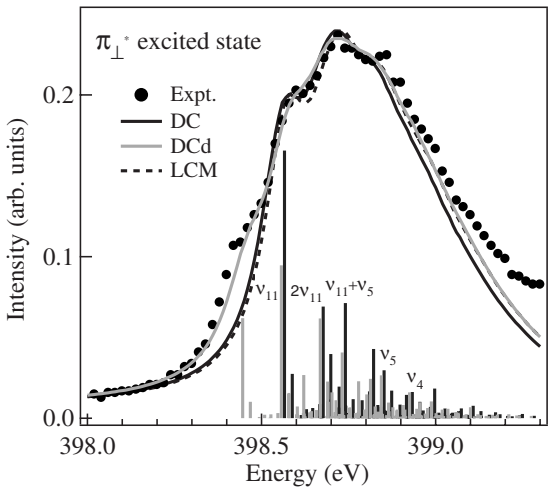

FIG. 6. Vibrational progression in the $\pi^*_\perp$-excited state calculated directly (full line) and using the LC model (dashed line). Black intensity bars correspond to the direct calculation (DC). Gray full line direct calculation with displacement (DCd) and intensity bars correspond to calculation including a shift of $\Delta q=+0.15$ of the $a=11$ potential, corresponding to C–C stretching. For the DCd simulation the character of the most important intensity (gray) bars is indicated.

monic probability, FC(1), is zero for all out-of-plane vibrations, for symmetry reasons, FC(2) will be taken as a measure of the excitation of each mode. There are nine modes with FC(2) different from zero. The most excited among them are C=C and C–C stretching and C=C torsion, followed by C≡N stretching and C–C≡N bending. This rich vibrational progression makes the $\pi^*_\perp$ structure much broader than can be predicted by only the experimental resolution.

The LC model gives approximately the same vibrational progression for in-plane modes. For very low frequency out-of-plane modes, the values of the FC factors calculated by the method of Katriel [23] are slightly overestimated, compared to the direct calculation.

Simulations done by both methods are shown in Fig. 6. Convolution was done with Lorentzian profiles with full width at half-maximum of 140 meV, the convolution between the experimental resolution (70 meV), and the typical lifetime broadening for N 1*s* core excitation (123 meV [6,43]) for the mean lifetime of the excited state. Intensity bars are given for the direct calculation. The most important intensity corresponds to the transition from $n=0$ to $n'=0$ for all modes, followed by two (C=C and C–C) monomode excitations. Direct calculation and the LC model give a very similar form, which matches well to experiment, particularly in the central part of the NEXAFS structure. However, the low-energy shoulder is not well reproduced.

Even if the experiment is done at room temperature, including thermic excitations in the initial state cannot explain the low-energy shoulder. The shoulder appears when a shift of $\Delta q=+0.15$ and $\Delta E=-0.12$ eV is applied to the potential curve of the C–C stretching mode ($a=11$). It creates an inversion of the first FC factors: FC(0) diminishes to 0.25 and FC(1) increases to 0.38. The gray line in Fig. 6 presents corrected vibrational progression, and gray intensity bars present the change in the distribution of multimode excitation probabilities. The need for this correction can be explained by the fact that the C–C shortening of 9.3 pm is the most important difference between the ground-state geometry and the optimized $\pi^*_\perp$-excited-state geometry. Moreover, the projection of the difference of the relaxed excited-state geometry and ground-state geometry to q_{11} gives $\Delta Q_{11}=0.43$. It is a relatively important value, compared to projections to other normal coordinates, which are less than 0.15. The minimum of the excited-state potential corresponding to the normal coordinate q_{11} is closer to its value in the excited optimized state than can be expected according to the developing of the multidimensional potential surface to rigid ground-state normal coordinates.

2. *Transition to the* $\pi^*_\parallel$(C≡N)

When a N 1*s* electron is promoted to a $\pi^*_\parallel$(C≡N) orbital, the electronic density of the $\pi^*_\perp$ orbital is shifted to the nitrogen atom [see Fig. 2(e)]. This density redistribution is, however, less important than that in the $\pi^*_\perp$-excited state. Density changes in the singly occupied $\pi^*_\parallel$ orbital are almost invisible [see Fig. 2(f)], because it is already located on the (C≡N) group, and its extra electron can participate in the core-hole screening.

The potential corresponding to the path joining the vertically attained (for $q=0$) and the geometry relaxed excited state is shown in Fig. 7, together with the modification of the molecular shape. Relaxed geometry has a zig-zag form and 1.13 eV lower energy. Compared to the $\pi^*_\perp$-excited state, relaxed interatomic distances are closer to those of the ground state: the N≡C distance is just 3% longer, the C–C distance is only 3% shorter, and the C=C distance is almost equal (see Table I). In contrast, angle changes are important,

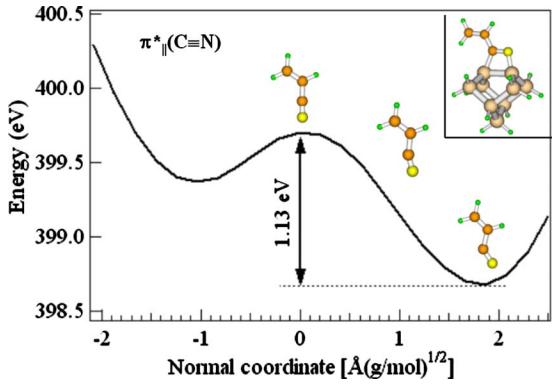

FIG. 7. (Color online) Potential leading to the optimized geometry in the $\pi_{\parallel}^{*}$-excited state, in the function of the normal coordinate distance between the $\pi_{\parallel}^{*}$-excited with ground-state molecular shape and relaxed geometry $\pi_{\parallel}^{*}$-excited state. The optimized geometry corresponds to the deeper minimum of the potential, and it has 1.13 eV lower energy than the vertically attained (at $q=0$) $\pi_{\parallel}^{*}$-excited state. Compared to the ground-state geometry, which has C−C≡N linear, it has 50° bending of the C−C≡N angle. A similar geometry, that of the acrylonitrile cycloadded to a dimer of a silicon (100) surface, represented here by a Si_9H_{12} cluster, is shown in the inset.

for the most important deformation is the 50° bending of the C−C≡N angle.

The relaxed $\pi_{\parallel}^{*}$ geometry is very close to the cycloaddition adsorbed acrylonitrile on a Si(100) surface [38–42], shown in the inset of Fig. 7. In the first case, it is an N 1*s* electron which is accommodated in the $\pi_{\parallel}^{*}$ orbital. In the second case, an electron of a Si-dimer dangling bond occupies the $\pi_{\parallel}^{*}$ orbital, participating in Si–C and Si–N σ bonding. Interatomic distances and angles are compared for the two cases in Table I. Forced to adapt to the Si–Si distance of a silicon dimer, in the case of cycloaddition, the C≡N distance is subjected to 0.1 Å (8%) extension. The relaxed geometry is as well similar to that of CH_2CHCHO, the acrylaldehyde molecule (see Fig. 8 and Table I). In this case, the $\pi_{\parallel}^{*}$ orbital is occupied by an electron shared with a supplementary hydrogen atom. Note that, in the three cases, accommodating the extra electron in the $\pi_{\parallel}^{*}$ orbital changes the hybridization of the C_1 atom from *sp* to sp^2, and thus affects the shape of the spinal column of the molecule.

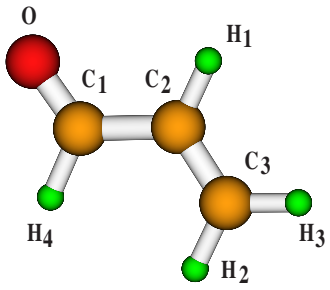

FIG. 8. (Color online) $O=C_1-C_2=C_3$ spinal column of the acrylaldehyde molecule has similar shape as the $N=C_1-C_2=C_3$ column of $\pi_{\parallel}^{*}$-excited acrylonitrile.

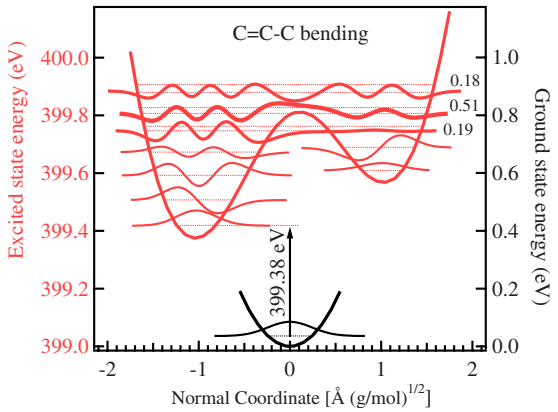

FIG. 9. (Color online) Ground state (black full line), $\pi_{\parallel}^{*}$-excited-state [gray (red) full line] potential, and corresponding wave functions, for the most excited, C=C−C bending, vibrational mode ($a=13$). Horizontal dashed lines indicate corresponding eigenvalues. The arrow indicates a vertical transition (at $q=0$) between ψ_0 and ψ_0'. The probability of the excitation of the most important quantum states is indicated, and these wave functions are drawn by a thicker line.

The $\pi_{\parallel}^{*}$(C≡N) excited-state potential surface developed in 15 normal modes of the ground state gives 12 single-well and two asymmetric-double-well potentials ($a=13$ and $a=15$ in-plane modes), and one symmetric-double-well potential with very small barrier (out-of-plane, $a=14$, mode).

The ground and the $\pi_{\parallel}^{*}$-excited-state potentials for the most excited, C=C−C bending, vibrational mode ($a=13$) are shown in Fig. 9 together with corresponding eigenvalues and eigenfunctions. The excited-state potential has an asymmetric-double-well form with two local minima out of the extension of the ground-state wave function. Overlap of the first vibrational quantum states of the excited state with the ground-state wave function is negligible. The FC factors are important only for even wave functions with eigenvalues close to the top of the barrier. Two of them exhibit tunneling effect across the potential barrier.

Table II ($\pi_{\parallel}^{*}$-excited state) presents the first vibrational quanta, the frequency change of the single-well modes, the quantum number of the most excited vibrational state, the first three FC factors for each mode, and the FC factor of the most excited state. Frequency change (less than 10%) of single-well modes is small compared to those of the $\pi_{\perp}^{*}$-excited state. FC(0) shows that the probability of ψ_0 to ψ_0' transition is the most important for all modes except for $a=13$ and $a=15$, with asymmetric-double-well potentials. For these modes, elevated vibrational quantum states are excited. The symmetric-double-well potential has as well FC(0) close to 1, because its barrier is lower than the $n'=0$ eigenvalue.

The LC model gives approximately the same vibrational progression for single-well modes, but highly underestimates $\mathcal{A}_{FC}(n\neq 0)$ factors for double-well modes. Their gradient of the excited potential [Eq. (9)] at $q=0$ is close to zero. Eliminating modes with double-well potentials, the LC model predicts essentially N≡C stretching excitation in the $\pi_{\parallel}^{*}$-excited state.

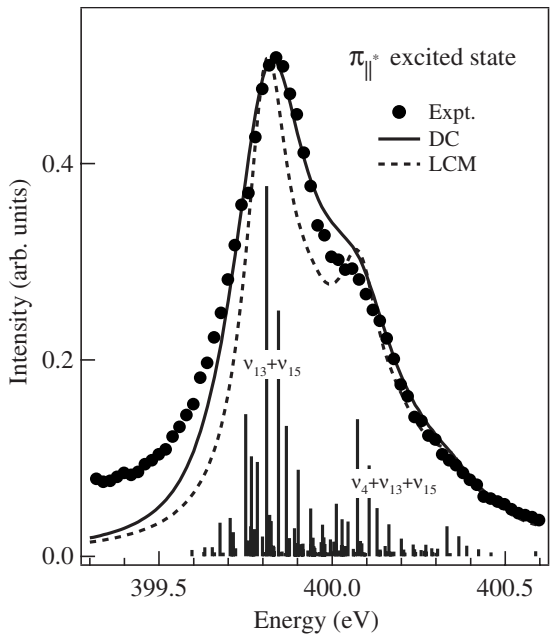

FIG. 10. Vibrational progression in the $\pi_{\|}^*$-excited state calculated directly (full line) and using the LC model (dashed line). Intensity bars higher than 10^{-3} are shown for direct calculation. Excitation character of the most important intensity bars is indicated: There is a group of bars at about 399.8 eV with different combinations of $a=13,15$ bimodal excitations, and a group at about 400.1 eV concerning $a=4,13,15$ trimodal excitations.

Figure 10 compares simulations done by direct calculation and using the LC model. The LC model predicts two resolved structures, the highest in energy corresponding mostly to the monomode N≡C stretching excitation. This is not in accordance with experiment, which shows just a high-energy shoulder. Direct calculation progression matches well to the experimental structure. It is broader, with smoother lines, due to excitations of elevated vibrational quantum states of bending modes, responsible for important multimodal excitations.

V. CONCLUSION

Vibrations excited by two N $1s\rightarrow\pi^*$ transitions of an acrylonitrile molecule are calculated directly by resolving the Schrödinger equation for each normal mode, and confronted to the linear coupling model. Direct calculation matches the experimental NEXAFS spectrum perfectly, as shown in Fig. 11. It reveals that nine vibrational modes are present in the $\pi_{\perp}^*$-excited state, corresponding to the N $1s\rightarrow\pi_{\perp}^*$(C=C−C≡N) transition. The most excited of them are the high frequency stretchings of bonds constituting the spinal column of the molecule, and the out-of-plane torsion of the C=C bond. Surprisingly, C≡N stretching is not the most excited

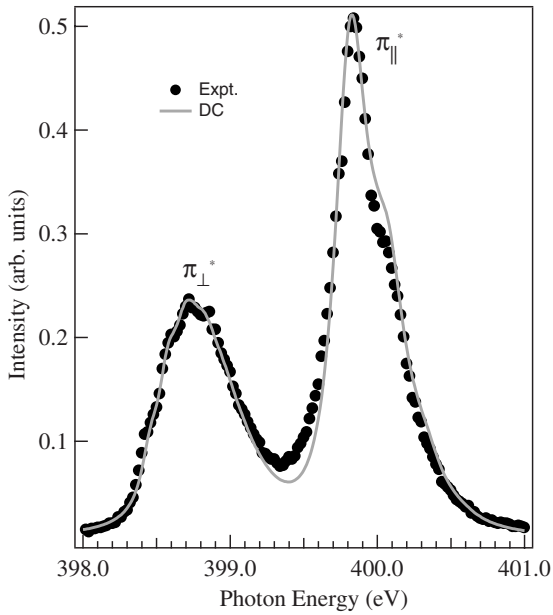

FIG. 11. Best simulations of two N $1s\rightarrow\pi^*$ excitations added and compared to the experiment.

mode. It is surpassed by C–C and C=C stretchings. This can be related to the delocalized character of the $\pi_{\perp}^*$(C=C−C≡N) orbital accommodating the core electron. This rich vibrational progression explains why the experimental $\pi_{\perp}^*$ NEXAFS structure is broader than expected from the experimental resolution.

As the $\pi_{\|}^*$(C≡N) orbital is localized on the C≡N bond, among six stretching modes the N $1s\rightarrow\pi_{\|}^*$ transition excites almost exclusively C≡N stretching. But accommodating the core electron in the $\pi_{\|}^*$(C≡N) orbital alters the hybridization of the C atom in the C≡N group from sp to sp^3, and the molecule tends to bend. Two in-plane low frequency bending modes (C=C−C and C−C≡N) are highly excited, making the $\pi_{\|}^*$ NEXAFS structure broad. Correct calculation of Franck-Condon factors for asymmetric-double-well potentials, particular to in-plane bending modes, can be done only by the direct method.

ACKNOWLEDGMENTS

The experimental work was supported by the EC Access to Research Infrastructures program. The authors also wish to thank the staff of the MAX laboratory for technical support and M. Huttula, R. Sankari, and J. Nikkinen for help with the experiment. Fruitful discussions with R. Taïeb are greatfully acknowledged. We are grateful for the generous allocation of time on the machines of the CNRS, particularly on cluster IBM SP (ZAHIR).

[1] M. Renier, T. Brochard, C. Nemoz, and W. Thomlinson, Nucl. Instrum. Methods Phys. Res. A **479**, 656 (2002).
[2] U. Gelius, E. Basilier, S. Svensson, T. Bergmark, and K. Siegbahn, J. Electron Spectrosc. Relat. Phenom. **2**, 405 (1973).
[3] R. Fink, J. Chem. Phys. **106**, 4038 (1997).
[4] R. Püttner, I. Dominguez, T. J. Morgan, C. Cisneros, R. F. Fink, E. Rotenberg, T. Warwick, M. Domke, G. Kaindl, and A. S. Schlachter, Phys. Rev. A **59**, 3415 (1999).
[5] S. J. Osborne *et al.*, J. Chem. Phys. **106**, 1661 (1997).
[6] J. Adachi, N. Kosugi, E. Shigemasa, and A. Yagishita, J. Chem. Phys. **102**, 7369 (1995).
[7] H. Köppel, F. X. Gadea, G. Klatt, J. Schrimer, and L. S. Cederbaum, J. Chem. Phys. **106**, 4415 (1997).
[8] Y. Ma, F. Sette, G. Meigs, S. Modesti, and C. T. Chen, Phys. Rev. Lett. **63**, 2044 (1989).
[9] D. Duflot, J.-P. Flament, I. C. Walker, J. Heinesch, and M.-J. Hubin-Franskin, J. Chem. Phys. **118**, 1137 (2003).
[10] K. C. Prince, R. Richter, M. Simone, M. Alagia, and M. Coreno, J. Phys. Chem. A **107**, 1955 (2003).
[11] S. Carniato, V. Ilakovac, J. J. Gallet, E. Kukk, and Y. Luo, Phys. Rev. A **70**, 032510 (2004).
[12] S. Carniato, V. Ilakovac, J. J. Gallet, E. Kukk, and Y. Luo, Phys. Rev. A **71**, 022511 (2005).
[13] M. Alagia, M. Lavollée, R. Richter, U. Ekström, V. Carravetta, D. Stranges, B. Brunetti, and S. Stranges, Phys. Rev. A **76**, 022509 (2007).
[14] M. Abu-samha, K. J. Børve, L. J. Sæthre, and T. D. Thomas, Phys. Rev. Lett. **95**, 103002 (2005).
[15] F. Halverson, R. F. Stamm, and J. J. Whalen, J. Chem. Phys. **16**, 808 (1948).
[16] M. Bassler, J.-O. Forsell, O. Björenholm, R. Feifel, M. Jurvansuu, S. Aksela, S. Sundin, S. L. Sorensen, R. Nyholm, A. Ausmees, and S. Svensson, J. Electron Spectrosc. Relat. Phenom. **101–103**, 953 (1999).
[17] S. Svensson *et al.*, Rev. Sci. Instrum. **67**, 2149 (1996).
[18] R. N. S. Sodhi and C. E. Brion, J. Electron Spectrosc. Relat. Phenom. **34**, 363 (1984).
[19] M. Wagner, Z. Naturforsch. A **14A**, 81 (1959).
[20] W. L. Smith, J. Phys. B **2**, 2 (1968).
[21] P. Macak, Y. Luo, and H. Ågren, Chem. Phys. Lett. **330**, 447 (2000).
[22] F. Ansbacher, Z. Naturforsch. A **14A**, 889 (1959).
[23] J. Katriel, J. Phys. B **3**, 1315 (1970).
[24] A. D. Becke, J. Chem. Phys. **98**, 5648 (1993).
[25] C. Lee, W. Yang, R. G. Parr, Phys. Rev. B **37**, 785 (1988).
[26] M. W. Schmidt *et al.*, J. Comput. Chem. **14**, 1347 (1993).
[27] B. Brena, Y. Luo, M. Nyberg, S. Carniato, K. Nilson, Y. Alfredsson, J. Åhlund, N. Mårtensson, H. Siegbahn, and C. Puglia, Phys. Rev. B **70**, 195214 (2004).
[28] F. Evangelista, V. Caravetta, G. Stefani, B. Jansik, M. Alagia, S. Stranges, and A. Ruocco, J. Chem. Phys. **126**, 124709 (2007).
[29] W. Kutzelnig, U. Fleisher, and M. Schindler, *The IGLOO-Method: Ab Initio Calculations and Interpretation of NMR Chemical Shifts and Magnetic Susceptibilities* (Springer-Verlag, Heidelberg, 1990), Vol. 23.
[30] R. Krishnan, J. S. Binkley, R. Seeger, and J. A. Pople, J. Chem. Phys. **72**, 650 (1980).
[31] T. Ziegler, A. Rauk, and E. J. Baerends, Theor. Chim. Acta **43**, 261 (1977).
[32] L. Triguero, O. Plashkevych, L. G. M. Petersson, and H. Ågren, J. Electron Spectrosc. Relat. Phenom. **104**, 195 (1999).
[33] *Landolt-Bornstein, Group II: Atomic and Molecular Physics*, edited by K. H. Hellwege and A. M. Hellwege (Springer-Verlag, Berlin, 1976), Vol. 7.
[34] *Handbook of Chemistry and Physics*, 74th ed., edited by D. R. Lide (CRC, Boca Raton, FL, 1993).
[35] M. Raynaud, J. Riga, C. Raynaud, and Y. Ellinger, J. Electron Spectrosc. Relat. Phenom. **53**, 251 (1991).
[36] F. Motte-Tollet, D. Messina, and M.-J. Hubin-Franskin, J. Chem. Phys. **103**, 80 (1995).
[37] M.-J. Hubin-Franskin, H. Aouni, D. Duflot, F. Motte-Tollet, C. Hannay, L. F. Ferreira, and G. Tourillon, J. Chem. Phys. **106**, 35 (1997).
[38] F. Tao, W. S. Sim, G. Q. Xu, and M. H. Qiao, J. Am. Chem. Soc. **123**, 9397 (2001).
[39] C. H. Choi and M. S. Gordon, J. Am. Chem. Soc. **124**, 6162 (2002).
[40] F. Bournel, J.-J. Gallet, S. Kubsky, G. Dufour, F. Rochet, M. Simeoni, and F. Sirotti, Surf. Sci. **513**, 37 (2002).
[41] M. Cobian, V. Ilakovac, S. Carniato, N. Capron, G. Boureau, R. Hirschl, and J. Hafner, J. Chem. Phys. **120**, 9793 (2004).
[42] M. Cobian, G. Boureau, J. Hafner, and G. Kresse, J. Chem. Phys. **123**, 174705 (2005).
[43] M. Coville and T. D. Thomas, Phys. Rev. A **43**, 6053 (1991).